

Elasto-dynamic analysis of a gear pump. Part IV: improvement in the pressure distribution modelling

E. Mucchi (*), G. Dalpiaz (*), A. Fernández del Rincón ()**

(*) Engineering Department, University of Ferrara
Via Saragat, 1 I-44122 Ferrara, Italy.

(**) Departamento de Ingeniería Estructural y Mecánica, University of Cantabria
E.T.S.I.I.T., Avda. Los Castros s/n, 39005 Santander, Spain.

Corresponding Author:

Emiliano Mucchi

Engineering Department, University of Ferrara

Via Saragat, 1 I-44122 Ferrara, Italy

email: emiliano.mucchi@unife.it

tel: +39 0532 974913

fax: +39 0532 974870

ABSTRACT

This work concerns external gear pumps for automotive applications, which operate at high speed and low pressure. In previous works of the authors (Part I and II,[1][2]), a non-linear lumped-parameter kineto-elastodynamic model for the prediction of the dynamic behaviour of external gear pumps was presented. It takes into account the most important phenomena involved in the operation of this kind of machine. Two main sources of noise and vibration can be considered: pressure period variation and gear meshing. The model has been used in order to foresee the influence of working conditions and design modification on vibration generation. The model experimental validation is a difficult task. Thus, Part III proposes a novel methodology for the validation carried out by the comparison of simulations and experimental results concerning forces and moments: it deals with the external and inertial components acting on the gears, estimated by the model, and the reactions and inertial components on the pump casing and the test plate, obtained by measurements. The validation is carried out comparing the level of the time synchronous average in the time domain and the waterfall maps in the frequency domain, with particular attention to identify system resonances. The validation results are satisfactory globally, but discrepancies are still present. Moreover, the assessed model has been properly modified for the application to a new virtual pump prototype with helical gears in order to foresee gear accelerations and dynamic forces. Part IV is focused on improvements in the modelling and analysis of the phenomena bound to the pressure distribution around the gears in order to achieve results closer to measured values. As a matter of fact, the simulation results have shown that a variable meshing stiffness has a notable contribution on the dynamic behaviour of

the pump but this is not as important as the pressure phenomena. As a consequence, the original model was modified with the aim at improving the calculation of pressure forces and torques. The improved pressure formulation includes several phenomena not considered in the previous one, such as the variable pressure evolution at input and output ports, as well as an accurate description of the trapped volume and its connections with high and low pressure chambers. The importance of these improvements are highlighted by comparison with experimental results, showing satisfactory matching.

KEYWORDS: External gear pumps; elastodynamic model; pressure ripples; pressure distribution; dynamic analysis; simulation results.

Nomenclature

Latin symbols

A	orifice section
B	length between the delivery sides of the relief grooves (see Figure 4a)
b_b	bearing block width
b_k	face width of gear k
B_{oil}	oil bulk modulus
$h_{b,i}$	radial clearance between the casing and the bearing block in correspondence of tooth space i
h_f	lateral clearance between bearing block and the lateral flank of the tooth
h_i	radial clearance between tooth tip i and the casing
l_t	tooth tip thickness
p	pressure in the generic control volume
p_{atm}	atmospheric pressure
p_d	pressure in the drainage circle (equal to p_{atm})
p_i	pressure in the tooth space volume i
p_{in}	pressure in the inlet volume
p_{out}	pressure in the outlet volume
p_t	pressure in the trapped volume
r_c	internal radius of the bearing block in the gear house
r_d	radius of the drainage circle
$r_{ext,k}$	outside radius of gears
r_m	radius at half height of the tooth
Q	volumetric flow rate
$Q_{b,i}$	axial volumetric flow rate through clearance $h_{b,i}$
$Q_{d,i}$	volumetric flow rate between isolated tooth space i and the drainage circle through clearance h_d
$Q_{d,t}$	volumetric flow rate between the trapped volume and the drainage circle

$Q_{f,i}, Q_{f,i+1}$	volumetric flow rate between isolated tooth spaces through clearance h_f
$Q_{f,t,in}, Q_{f,t,out}$	volumetric flow rate between the trapped volume and the inlet and outlet volumes through clearance h_f
$Q_{h,i}, Q_{h,i+1}$	volumetric flow rate between isolated tooth spaces through clearances h_i, h_{i+1}
$Q_{T,in,atm}$	turbulent volumetric flow rate between the inlet volume and the reservoir
$Q_{T,out,atm}$	turbulent volumetric flow rate from the outlet volume to the hydraulic circuit
$Q_{T,t,in}, Q_{T,t,out}$	turbulent volumetric flow rate between the trapped volume and the inlet and outlet volumes, respectively
t	time
V	volume of the generic control volume
V_i	volume of the tooth space i
V_{in}, V_{out}	volumes of the inlet and outlet volumes
V_t	volume of the trapped volume
$V_{t0}, V_{in0}, V_{out0}$	values of the trapped volume, inlet volume and outlet volume when $\theta = 0$, i.e. in the initial condition when the second contact begins

Greek symbols

ΔQ	difference between the volumetric flow rates, coming into a control volume and coming out
θ	angular coordinate
$\theta_a, \theta_b, \theta_{t,end}$	angles defining the beginning of the connection with the inlet volume, the end of the connection with the outlet volume and the end of the trapped volume, respectively (see Figure 4b)
μ	Oil dynamic viscosity
ρ	oil density
ω	angular speed

Subscripts

i	denotes tooth space
$k=1,2$	denotes gears
n,m	number of isolated tooth spaces in gear 1 and 2, respectively
$ _k$	applied to gear k

1. INTRODUCTION

External gear pumps exhibit a complex interrelationship between gear meshing, clearances between components and pressure pulsation that makes difficult the definition of general design procedures. As a consequence, large amounts of time and money are spent during the development of new designs. This requires huge testing efforts in order to refine the noise and vibration behaviour and simultaneously achieve good hydraulic efficiency. A good dynamic model could be a useful and powerful tool for the identification of noise and vibration sources and design improvement allowing “Design Right First Time” which leads to shorter time-to-market and reduced costs as compared to conventional “Test, Analyze & Fix”. Following this objective, in Part I and II ([1][2]), the authors have presented a numerical model for the dynamic analysis of an external gear pump for automotive applications (called hereafter *PModel*). Fluid pressure distribution around the gears, which is time-varying, is computed and included as a resultant external force and torque

acting on each gear. Gear meshing phenomena have received particular attention, the time-varying meshing stiffness [3] and the tooth profile errors, the effects of the backlash between meshing teeth, the oil squeeze and the possibility of tooth contact on both contact lines have been included in the model. One of the particular features of gear pump design is the use of hydrodynamic journal bearings for gear shaft support. The non-linear dynamics of this kind of bearings has been modelled using the theory of Childs [4] called “finite impedance formulation”. The experimental validation carried out in Part III, can be considered rather good, but not completely satisfactory requiring a model refinement in order to improve the correlation between experimental and simulated results.

The simulation results show that the developed model makes it possible to estimate dynamic responses and forces taking place in the gear pumps, as a function of working conditions. One of the vibration sources is the variable meshing stiffness. However, on the basis of numerical simulations it gives a minor contribution to the final results (see also Section 6.2 of the Part III). On the other hand, pressure forces and torques show the most important variations due to the change in the number of isolated volumes carrying fluid and to the creation of a “trapped volume” between two consecutive tooth pairs in contact. Furthermore, gear pumps exhibit pressure ripple in the pressure evolution trend during a complete gear rotation [5-14]. The pressure ripple can determine oscillating forces within the system leading to vibration and noise generation. As a consequence, the original model (*PModel*) was modified with the aim of improving the calculation of the pressure distribution, pressure forces and torques in order to achieve a behaviour closer to the real measurements. In this sense, the new model (called hereafter *NModel*) includes an improved pressure formulation with several phenomena not considered in the *PModel*; these include: the pressure variations in the input and output chambers, the axial flows through the clearances between floating bearing blocks and casing as well as an accurate description of the trapped volume and its connections with high and low pressure chambers. The pressure formulation of the trapped volume has been completely reformulated avoiding the previous assumption of a linear pressure transition from the high to the low pressure [1]. Now, the flow areas between the trapped volume, input and output chambers are obtained numerically allowing the formulation of more complex relief groove designs. The pressure evolution around the gears is then calculated solving simultaneously the continuity equations of all the control volumes, following the procedure presented in the next section. This procedure requires the numerical integration of a non-homogeneous variable-dimension differential equation system that has been solved for each gear centre position. Therefore, a high computational effort is required for each integration step in the dynamic model. With the aim of reducing the integration time, the pressure distribution as well as the pressure forces and torques have been calculated in the gear ‘static’ equilibrium position instead of in the actual position along the centreline trajectory. In steady-state operational conditions, the gear centreline trajectory is an orbit around an eccentric position with respect to the casing.

This eccentric position is not the actual gear axis position, but it can be considered as a reference position during the axis orbital motion. It is hereafter referred as ‘static’ equilibrium position (SEP). In Part II [2] it has been verified that this approximation leads to negligible imprecision. Furthermore, the pressure forces and torques are evaluated by using an improved formulation with respect to that implemented in the previous model.

The contents of this Part IV are as follows. Section 2 presents the improved formulation of the pressure distribution highlighting the phenomena not considered in the previous one, such as the axial flow (Section 2.1), the accurate description of the trapped volume and its connections with high and low pressure chambers (Sections 2.2), the pressure variations in the input and output chambers (Sections 2.3) and the variable dimension equation system (Section 2.4). The improved procedure for the pressure force and torque evaluation is presented in Section 3. Section 4 addresses the new experimental validation and presents several simulation results. In particular, in Section 4.1 the improved model is experimentally assessed by using the same methodology used in Part III. In Section 4.2, the simulation results consenting the pressure evolution in a control volume for a complete gear rotation estimated by using the previous and the new model are compared as well as the pressure forces and torques. Eventually, Section 5 is devoted to concluding remarks.

2 PRESSURE DISTRIBUTION:IMPROVED FORMULATION

The pressure increase in the travel from the low to the high pressure region is more or less progressive but is really conditioned by several dimensional and operational parameters as the clearances in the radial and axial direction, oil viscosity, output pressure and shaft speed. In order to study the pressure variation and following the Euler’s approach, the pump is divided into several “control volumes”. In the case being studied, the considered volumes (see Figure 1a) are each isolated tooth space (V_i), the inlet and outlet chambers (V_{in} , V_{out}) and the volume between meshing teeth (V_t , called “trapped volume”). Applying the continuity equation and the state equation of the fluid to a generic control volume, assuming an adiabatic and isentropic transformation, the following relation expressed in terms of gear angular coordinate θ is obtained [5] [6] [16]:

$$\frac{dp}{d\theta} = \frac{B_{oil}}{V\omega} \left(\Delta Q - \frac{dV}{d\theta} \omega \right) \quad (1)$$

Eq. (1) allows the calculation of the pressure variation of a fluid (characterized by the oil bulk modulus B_{oil}) contained in the control volume V , caused by the volumetric flow rate gain ΔQ and by the volume variation $dV/d\theta$. The expressions of the terms on the right side of Eq. (1), i.e. volume V , its variation $dV/d\theta$ and flow rate gain ΔQ , have to be determined for each control volume. Thus, it is necessary to understand how each volume communicates with the others through the clearances of the pump in order to estimate these flow rates. Figure 1 shows these volumes and their relationships. The arrows in Figure 1b depict the direction of the flows exchanged between the volumes. It can be noted that the number of the control volumes is variable during the gear rotation because of the variation of the number of isolated tooth spaces between the gears and the casing and because the trapped volume exists only when there are two meshing contacts. The changes in number of control volumes are due to:

- appearance of a new tooth space volume on gear 1, during the period $\theta_2 \rightarrow \theta_4$
- disappearance of a tooth space volume on gear 1, during the periods $\theta_4 \rightarrow \theta_p, \theta_0 \rightarrow \theta_2$
- appearance of a new tooth space volume on gear 2, during the periods $\theta_0 \rightarrow \theta_1, \theta_5 \rightarrow \theta_p$
- disappearance of a tooth space volume on gear 2, during the period $\theta_1 \rightarrow \theta_5$
- appearance of the trapped volume, during the period $\theta_0 \rightarrow \theta_3$
- disappearance of the trapped volume, during the period $\theta_3 \rightarrow \theta_p$

Table 1 summarizes the changes in the number of control volumes within the integration interval, i.e. during an angular pitch θ_p . The equation integration is performed for a gear rotation equal to the angular pitch. The starting position in the integration of the equation system is when a new meshing begins. So, a variation in the number of control volumes causes a change in the number of differential equations that have to be integrated in order to obtain the pressure distribution. For that reason it is not possible to perform only one integration using as integration interval the duration of an angular pitch, but six integrations have to be done (one for each column of Table 1). In the following, for the four different kinds of control volumes (isolated tooth spaces, trapped volume, inlet chamber and outlet chamber) each term of Eq. (2) will be calculated. In particular the flow rates will be calculated taking into account the contribution of the pressure drop between adjacent volumes and the “drag” flow. It is well-known that for a fluid film element with height h , length l and width w , the volumetric flow rate due to the pressure drop Δp can be calculated using the Poiseuille’s equation that supposes laminar flow:

$$Q_p = \frac{wh^3}{12\mu} \frac{\Delta p}{l} \quad (2)$$

On the other hand, the volumetric “drag“ flow rate has a linear distribution from zero to u , where u is the relative velocity of the upper part of the fluid film element with respect to the bottom part and can be calculated using the well-known relation:

$$Q_u = \frac{wuh}{2} \quad (3)$$

Relations (2) and (3) will be used in the following in order to calculate flow rate gain ΔQ in the four kinds of control volumes while volume variation $\frac{dV}{d\theta}$ is obtained from geometrical considerations. Once the flow rate gain and the volume variation are obtained for all the control volumes, the resulting equation system can be numerically integrated in order to obtain the pressure distribution around the gears. In the following, Eq. (1) will be used for the evaluation of the pressure in the tooth spaces around the gears (Section 2.1), in the trapped volume (Section 2.2), in the inlet and outlet chambers (Section 2.3).

2.1 Continuity equation for a generic tooth space

Figure 2a shows the generic tooth space “ i ”, edged between two consecutive tooth flanks (i and $i+1$) and the casing. Each tooth space is connected (see also Figure 1b and Figure 2b) with the adjacent tooth spaces by the corresponding clearances between casing and tooth tip (h_i , h_{i+1}) and between the bearing blocks and the tooth lateral flanks (h_f). In addition, it is connected with the drainage circle through clearance h_f , and lastly with the low or high pressure through the clearances $h_{b,i}$ between the bearing blocks and the casing in axial direction. So, Eq.(1) applied to the generic tooth space “ i ” becomes:

$$Q_{h,i+1} - Q_{h,i} + 2(Q_{f,i+1} - Q_{f,i}) - 2Q_{d,i} - 2Q_{b,i} = \left(\frac{V_i}{B_{oil}} \frac{dp_i}{d\theta} + \frac{dV_i}{d\theta} \right) \omega_k \quad (4)$$

It can be noted that the flows through clearances h_f and $h_{b,i}$ are double because there are two sides for each gear and symmetry is assumed. Flow rates $Q_{h,i}$, $Q_{f,i}$, $Q_{d,i}$ and $Q_{b,i}$ are taken as positive coming out of the tooth space i , while $Q_{f,i+1}$ and $Q_{h,i+1}$ are considered as positive when coming into tooth space i . Applying Eqs. (2) and (3) to the **passageway on the tooth tip** it is possible to calculate the volumetric flow rate in the tooth space i , taking into account the pressure drop contribution as well as the drag flow rate (due to the relative motion of the gear with respect to the casing):

$$Q_{h,i} = \frac{b_k h_i^3}{12 \mu l_t} (p_i - p_{i-1}) + \frac{b_k \omega_k r_{ext} h_i}{2} \quad (5)$$

The height of clearance h_i between the tooth tip and the casing depends on the position of the gear shaft (because of the eccentricity of the gear with respect to the casing) and on the casing wear. So, the radial clearance will be different for each tooth along the gear, (more details can be found in [1]). The volumetric flow rate between the lateral bearing blocks and the lateral flank of the tooth ($Q_{f,i}$) can be estimated using an expression similar to Eq. (5). Average values for the passageway dimensions (h, l of Eqs (2) and (3)) have been considered since they are not geometrically defined and the relative velocity in the drag flow rate contribution is the velocity at half height of the tooth ($u_f = \omega_k r_m$). In particular, one can consider b_f as the height of the tooth and l_f as the thickness of the tooth measured of the pitch circle, leading to obtain:

$$Q_{f,i} = \frac{b_f h_f^3}{12 \mu l_f} (p_i - p_{i-1}) + \frac{b_f \omega_k r_m h_f}{2} \quad (6)$$

The drainage flow rate for tooth space i is given by the Poiseuille's equation, Eq. (2), assuming the passageway width b_d equal to 0.4 to 0.5 times the pitch on the root circle and the passageway length l_d the difference between the radius of the root circle and the radius of the drainage circle. In this case, the term relating to the drag flow rate has been neglected because its radial component is zero. Therefore, the volumetric flow rate becomes:

$$Q_{d,i} = \frac{b_d h_f^3}{12 \mu l_d} (p_i - p_d) \quad (7)$$

The bearing blocks were hydraulically balanced because they are subjected to axial forces due to the pressure distribution. The equilibrium of the bearing blocks was actuated by applying the high or low pressures on different parts of the same surface using a seal in order to divide the area where the low pressure acts with respect to the area where the high pressure acts (see Figure 3). Because of the clearance between the bearing block and the casing, the tooth space is put in communication (in the axial sense) with these low or high pressure areas depending on the position of the tooth space. With reference to Figure 3, if the tooth space is before point P, the tooth space will be connected with the low pressure; if it is beyond point P, the tooth space will be connected with the high pressure. Eventually the tooth space communicates with low and high pressure when point P is within the tooth spaces. So if the tooth space is connected with the low pressure chamber, the flow comes out of the tooth space; on the contrary, if the tooth space is connected with the high pressure chamber, the flow comes into the tooth space. Therefore, neglecting the term relating with the entrained flow, the axial flow rate becomes:

$$Q_{b,i} = \frac{r_c \theta_p h_{bm,i}^3}{12 \mu b_b} \Delta p_{b,i} \quad (8)$$

where :

$$\Delta p_{b,i} = \begin{cases} p_{out} - p_i & \text{beyond point P} \\ p_{in} - p_i & \text{before point P} \\ p_{mean} - p_i & \text{P within tooth space i} \end{cases} \quad \text{and} \quad h_{bm,i} = \frac{h_{b,i} + h_{b,i+1}}{2} \quad (9)$$

The height of clearance $h_{b,i}$ depends on the position of the bearing block, since they are floating and on the position of the gear into the journal bearings (SEP). It is very difficult to estimate the dynamic behaviour of the floating bearing blocks, for that reason let us suppose that the pressure distribution around the bearing blocks is the same as around the gears. Therefore, the bearing blocks will be subjected to a global pressure force that pushes them in a static position with zero backlash at the low pressure side. The height of clearance $h_{b,i}$ is evaluated on the basis of this assumption.

The last term to be calculated in Eq. (4) is volume variation dV_i . Such a term can be obtained for an angle rotation $d\theta$ of the gear with geometrical considerations by the relation:

$$\frac{dV_i}{d\theta} = r_{ext} b_k (h_{i+1} - h_i) \quad (10)$$

So, taking into account all the previous terms and substituting in Eq. (5), considering volume V_i as constant and equal to the nominal volume of the tooth space, the following equation for the generic tooth space i can be obtained:

$$\frac{dp_i}{d\theta} = \frac{B_{oil}}{\omega_k V_i} \left[C_h (h_{i+1}^3 \Delta p_{i+1} - h_i^3 \Delta p_i) - K_h (h_{i+1} - h_i) + 2C_f (\Delta p_{i+1} - \Delta p_i) - 2C_d \Delta p_{d,i} - 2C_b \Delta p_{b,i} \right] \quad (11)$$

where

$$C_h = \frac{b_k}{12\mu l_i}, \quad C_f = \frac{b_f h_f^3}{12\mu l_f}, \quad C_d = \frac{b_d h_d^3}{12\mu l_d}, \quad C_b = \frac{r_c \theta_p h_{bm,i}^3}{12\mu b_b}$$

$$\Delta p_{i+1} = p_{i+1} - p_i, \quad \Delta p_{d,i} = p_i - p_d, \quad \Delta p_i = p_i - p_{i-1},$$

$$V_i = V_0 \quad \forall i, \quad \frac{dV_i}{d\theta} \omega_k = 2K_h (h_{i+1} - h_i) \quad K_h = \frac{b_k \omega_k r_{ext}}{2}.$$

Eq. (11) is a differential equation that can be expressed as

$$\frac{dp_i}{d\theta} = f_i(p_{i-1}(\theta), p_i(\theta), p_{i+1}(\theta), p_{in}(\theta), p_{out}(\theta)) \quad (12)$$

where f_i is the function of the right side of Eq. (11).

2.2 Continuity equation for the trapped volume

The trapped volume exists only when two tooth pairs are meshing, therefore the continuity equation for the trapped volume will be taken into account only when the trapped volume exists. With reference to Figure 4, the trapped volume

is connected with the inlet volume, with the outlet volume and with the drainage circle through the clearance h_f and furthermore with the inlet and outlet volumes through the relief grooves. So, Eq. (1) applied to the trapped volume becomes:

$$-2Q_{T,t,out} - 2Q_{T,t,in} - 2Q_{f,t,in} - 2Q_{f,t,out} - 4Q_{d,t} = \left(\frac{V_t}{B_{oil}} \frac{dp_t}{d\theta} + \frac{dV_t}{d\theta} \right) \omega_k \quad (13)$$

It can be noted that several flow rates in Eq. (13) are double because the gear has two sides. Moreover, flow rate $Q_{d,t}$ is multiplied by 4 because there are two sides for each gear. Flow rates $Q_{f,t,in}$, $Q_{f,t,out}$, $Q_{d,t}$ through clearance h_f can be calculated using expressions similar to Eqs.(6) and (7) hypothesizing laminar flow:

$$Q_{f,t,in} = C_f (p_t - p_{in}) + \frac{b_f \omega_k r_m h_f}{2} \quad Q_{f,t,out} = C_f (p_t - p_{out}) + \frac{b_f \omega_k r_m h_f}{2} \quad (14)$$

$$Q_{d,t} = C_d (p_t - p_d) \quad (15)$$

As before, the term related to the entrained flow in drainage flow rate $Q_{d,t}$ has been neglected because its radial component is zero. It could happen, for example, that the pressure inside the trapped volume is less than the pressure in the outlet volume; in this scenario the oil flows into the trapped volume and thus, the flow rate changes its sign (since $p_t - p_{out} < 0$) and becomes negative. The flow through the relief grooves has to be considered as turbulent flow due to the connection orifice dimension and shape. Thus, the volumetric flow rate can be calculated using the well-known relation [16]:

$$Q = C_{flow} A \sqrt{\frac{2\Delta p}{\rho}} \quad (16)$$

where A is the area of the connection and C_{flow} is the flow coefficient (also called hydraulic resistance, see [17]) depending on Reynolds number and on the orifice dimension and shape. Therefore, the turbulent flow rates exchanged between the trapped volume and the inlet and outlet volumes are, respectively:

$$Q_{T,t,in} = \begin{cases} +0.65A_{in}\sqrt{\frac{2(p_t - p_{in})}{\rho}} & \text{if } p_t > p_{in} \\ -0.65A_{in}\sqrt{\frac{2|p_t - p_{in}|}{\rho}} & \text{if } p_t < p_{in} \end{cases} \quad Q_{T,t,out} = \begin{cases} +0.65A_{out}\sqrt{\frac{2(p_t - p_{out})}{\rho}} & \text{if } p_t > p_{out} \\ -0.65A_{out}\sqrt{\frac{2|p_t - p_{out}|}{\rho}} & \text{if } p_t < p_{out} \end{cases} \quad (17)$$

where the connection areas with the inlet and outlet volumes have been geometrically calculated as a function of gear rotational angle θ . Figure 4b shows the area variation during the gear rotation for the connection between the trapped volume and the inlet and outlet volumes. Starting from the position when two tooth pairs are in contact, the connection area with the outlet volume decreases till θ_b when the connection disappears, while the connection with the inlet volume begins in θ_a . It can be noted that from θ_a to θ_b the trapped volume is in communication both with the inlet and outlet volumes. Since the area and shape of the connections are variable, the calculus of the flow coefficient is not easy, therefore averaged values between similar kinds of connections have been taken into account [17]. The last two terms to be calculated in Eq. (13) are volume V_t and its variation dV_t . Taking with reference Figure 5a, the trapped volume (when exists) is edged by $\overline{O_1CO_2D}$ and its variation takes the form:

$$dV_t = \frac{1}{2}(r_1^2(t+T) - r_1^2(t) - r_2^2(t) + r_2^2(t+T))b_k d\theta \rightarrow \frac{dV_t}{d\theta} = \frac{1}{2}(r_1^2(t+T) - r_1^2(t) - r_2^2(t) + r_2^2(t+T))b_k \quad (18)$$

where r_1, r_2 define the positions of the two tooth pairs in contact (the expression of r_1, r_2 as a function of the gear parameters can be found in [2]). Then, the volume of the trapped volume is obtained by integration of Eq. (18):

$$V_t(\theta) = V_{t0} + \int_0^{\bar{\theta}} \frac{dV_t}{d\theta} d\theta \quad (19)$$

The integration is performed when the trapped volume exists, i.e. in the angular interval 0 to $\theta_{t,end}$ (see Figure 4b); V_{t0} is the initial value of the trapped volume, which is geometrically calculated by the reconstruction of the gear geometry and $\bar{\theta}$ represents a generic angular position in the above interval. Substituting all the volumetric flow rates calculated above (Eqs. (14), (15) and (17)) and relation (18) describing the volume variation in Eq. (13) and reorganizing, the following relation similar to Eq. (12) can be obtained:

$$\frac{dp_t}{d\theta} = f_t(p_{in}(\theta), p_{out}(\theta), p_t(\theta)) \quad (20)$$

where f_t is a function of pressure in the outlet, inlet and trapped volumes.

2.3 Continuity equation for the inlet and outlet volumes

The inlet chamber communicates with the reservoir, with the drainage circle, with the first isolated tooth space of gear 1 and 2 through the clearance at the tooth tip h_t and through the lateral clearance h_f and finally with the trapped volume through the lateral clearance h_f and through the relief grooves, see Figure 1b and Figure 5b. Therefore, Eq.(1) applied to the inlet volume becomes:

$$Q_{T,in,am} + Q_{h,1}|_1 + Q_{h,1}|_2 + 2Q_{f,1}|_1 + 2Q_{f,1}|_2 + \sum_{i=1}^n Q_{d,i}|_1 + \sum_{i=1}^m Q_{d,i}|_2 + 4Q_{dt} + 2Q_{f,t,in} + 2Q_{T,t,in} = \left(\frac{V_{in}}{B_{oil}} \frac{dp_{in}}{d\theta} + \frac{dV_{in}}{d\theta} \right) \omega_k \quad (21)$$

The flow exchanged with the reservoir ($Q_{T,in,am}$) can be considered as a turbulent flow because of the orifice area and an expression similar to Eq.(16) could be used for the estimation of the flow rate. In such a case, flow coefficient C_{flow}

has been considered equal to 0.65, as suggested in [17], and $\Delta p = p_{in} - p_{amb}$ as pressure drop. The other flow rates in Eq. (21) have already been calculated for the continuity equations of the generic tooth space i (Section 2.1) and for the trapped volume (Section 2.2). In particular the flow rates with the isolated tooth spaces can be calculated using Eqs. (5) and (6) applied to the first isolated tooth space ($i = 1$) of gears 1 and 2. Moreover, since the drainage circle communicates with the inlet chamber, the drainage flow rates (Eqs. (7) and (15)) of all the tooth spaces ($i = 1 \dots n$ for gear 1 and $i = 1 \dots m$ for gear 2) and of the trapped volume finally pour into the inlet chamber. For this reason, all the drainage flow rates also appear in the continuity equation of the inlet volume. With reference to Figure 5a, the control volume for the inlet chamber is edged by $\overline{AO_1CO_2B}$; the variation of such a volume as a function of the angular rotation can be calculated using an expression similar to Eq.(18):

$$\frac{dV_{in}}{d\theta} = \frac{1}{2} \left(r_{ext,1}^2 + r_{ext,2}^2 - r_1^2(t+T) - r_2^2(t+T) \right) b_k, \quad (22)$$

while the volume of the inlet chamber is obtained by integration of Eq. (22):

$$V_{in}(\theta) = V_{in0} + \int_0^{\bar{\theta}} \frac{dV_{in}}{d\theta} \cdot d\theta \quad (23)$$

As done for the generic tooth space and for the trapped volume, Eq.(21) can be rearranged into the following form, substituting the above volumes and flow rates:

$$\frac{dp_{in}}{d\theta} = f_{in}(p_i(\theta), p_{in}(\theta), p_{out}(\theta), p_t(\theta)) \quad \begin{array}{ll} i = 1 \dots n & \text{for gear 1} \\ i = 1 \dots m & \text{for gear 2} \end{array} \quad (24)$$

When the pump is used in the steering system of vehicles, the outlet volume is connected through a valve to an oleodynamic actuator. This valve controls the pressure inside the pump tuning the orifice section. For this reason, the connection with the hydraulic circuit outside the pump through this valve has been modelled assuming turbulent flow by using Eq. (16). In order to estimate the coefficient $K_{out} = C_{flow} A$ in Eq. (16), the theoretical flow rate (namely Q_{th}) through the valve is used:

$$K_{out} = Q_{th} \sqrt{\frac{\rho}{2(p_{out} - p_{atm})}} \quad (25)$$

The theoretical flow rate (expressed in mm³/s) used in Eq. (25) is defined as $Q_{th} = C_v \omega_k / 2\pi$, where the volumetric capacity C_v is expressed in mm³/rev and the rotational speed ω_k in rad/s. The volumetric capacity is the volume of fluid that the pump can impel during a complete gear rotation; it is determined by geometric characteristics and neglecting leakage [10]. Then, coefficient K_{out} is used during the simulation for the evaluation of the turbulent flow rate thought out the valve (namely $Q_{T,out,atm}$ in Figure 6). Moreover, the outlet volume is connected to the last isolated tooth space of gear 1 and 2 through tooth tip clearance h_t and through lateral clearance h_f and finally with the trapped

volume (when it exists) through lateral clearance h_f and through the relief grooves. Therefore, Eq. (1) applied to the outlet volume becomes:

$$-Q_{T,out,atm} - Q_{h,n}|_1 - Q_{h,m}|_2 - 2Q_{f,n}|_1 - 2Q_{f,m}|_2 + 2Q_{f,t,out} + 2Q_{T,t,out} = \left(\frac{V_{out}}{B_{oil}} \frac{dp_{out}}{d\theta} + \frac{dV_{out}}{d\theta} \right) \omega \quad (26)$$

where the terms in the right side of the equation have already been calculated in the other control volumes and the outlet volume variation is defined as (see Figure 5a):

$$\frac{dV_{out}}{d\theta} = -\frac{1}{2} \left(r_{ext,1}^2 + r_{ext,2}^2 - r_1^2(t) - r_2^2(t) \right) b_k \quad (27)$$

Eq.(26) can be reorganized in the following form, as for the other control volumes:

$$\frac{dp_{out}}{d\theta} = f_{out} (p_n(\theta), p_{n-1}(\theta), p_m(\theta), p_{m-1}(\theta), p_{out}(\theta), p_t(\theta)) \quad (28)$$

2.4 Variable dimension equation system

Applying Eq. (12) to the n isolated volumes of gear 1 and to the m isolated volumes of gear 2 and joining such equations to the continuity equations for the remaining control volumes (Eqs. (20), (24) and (28)), a system of differential equations can be obtained and the unknown quantities, i.e. the pressure in the control volumes, can be calculated:

$$\left\{ \begin{array}{l}
\frac{dp_{in}}{d\theta} = f_{in}(p_i(\theta), p_{in}(\theta), p_{out}(\theta), p_t(\theta)) \\
\hline
\frac{dp_1}{d\theta} \Big|_1 = f_1(p_{in}(\theta), p_1(\theta), p_2(\theta), p_{out}(\theta)) \Big|_1 \\
\vdots \\
\frac{dp_n}{d\theta} \Big|_1 = f_n(p_{n-1}(\theta), p_n(\theta), p_{out}(\theta)) \Big|_1 \\
\hline
\frac{dp_1}{d\theta} \Big|_2 = f_1(p_{in}(\theta), p_1(\theta), p_2(\theta), p_{out}(\theta)) \Big|_2 \\
\vdots \\
\frac{dp_m}{d\theta} \Big|_2 = f_m(p_{m-1}(\theta), p_m(\theta), p_{out}(\theta), p_{in}(\theta)) \Big|_2 \\
\hline
\frac{dp_{out}}{d\theta} = f_{out}(p_n(\theta), p_{n-1}(\theta), p_m(\theta), p_{m-1}(\theta), p_{out}(\theta), p_t(\theta)) \\
\hline
\frac{dp_t}{d\theta} = f_t(p_{in}(\theta), p_{out}(\theta), p_t(\theta))
\end{array} \right. \quad (29)$$

In order to solve the equation system (29), an initial value of the pressure distribution in the first integration interval (θ_0 , see Table 1) has to be known. For that reason the pressure values obtained at the end of one integration step are used as initial values for a new integration cycle. After several cycles the solution for the pressure distribution is obtained. As an example of simulation result, Figure 7 shows the pressure evolution in a tooth space for a complete rotation of the two gears.

3. PRESSURE FORCES AND TORQUES: IMPROVED FORMULATION

3.1 Pressure forces

Once the pressure distribution for a complete rotation of the gears has been obtained, the resultant pressure force and the resultant pressure torque for each gear can be calculated. The formulation for estimating the pressure forces is different with respect to the previous formulation presented in Part I ([1]). In particular this formulation considers the tooth spaces in which the resultant pressure force in tangential direction is null (called hereafter “balanced tooth spaces”) and the tooth space where the resultant pressure force in tangential direction is not null (called hereafter “not balanced space”). It can be noted that the formulation concerning the calculus of the pressure forces in the balanced tooth spaces is not presented hereafter because such a formulation is the same as in the PModel (see Eqs. 22-24 in [1]): the pressure force was calculated as the vector sum of the pressure around the gear multiplied by the involved area. The original formulation presented hereafter concerns the unbalanced tooth space depicted in Figure 8, where r_k ($k=1,2$

denotes gears) defines the position of the meshing contact P in which the contact takes place (the expressions of r_k for both gears are defined in Eqs. 19-20 of [2]); in this tooth space the global tangential force is not null. The pressure force is firstly calculated in the local reference frame of the tooth space $O_k \overline{X}_k \overline{Y}_k$, with \overline{Y}_k -axis coincident with the symmetric axis of the tooth space and \overline{X}_k orthogonal. Then, the pressure force is reduced in the reference frame $O_k X_k Y_k$ of Figure 1a. When the meshing contact takes place in P, the tooth space surface becomes separated into two zones at different pressures: \overline{QP} at the inlet pressure and \overline{PR} at the outlet pressure. In order to simplify the pressure force calculation, the tooth space surface can be further split into three zones \overline{QP} , \overline{PS} , \overline{SR} and thus, the global pressure force can be obtained as the sum of the pressure force acting in each zone. The pressure force acting on balanced zone \overline{PS} has only radial component and it is equal to the pressure force acting on circumferential arc \overline{PS} :

$$f_{\overline{PS}} = 2p_{out} \sin\left(\frac{\theta_p - 2\theta_r}{2}\right) b_k r_k \quad (30)$$

The pressure force acting on tooth space surface \overline{SR} has both the radial and tangential component; the radial component, as above, is equal to the pressure force acting on circumferential arc $\overline{R'R}$, while the tangential component is equal to the pressure force acting on straight segment $\overline{R'S}$:

$$\begin{aligned} f_{\overline{R'R}} &= 2p_{out} \sin\left(\frac{\theta_r}{2}\right) b r_{ext} \\ f_{\overline{R'S}} &= p_{out} (r_{ext} - r_k) b \end{aligned} \quad (31)$$

In $O_k \overline{X}_k \overline{Y}_k$ reference frame such forces become:

$$\begin{cases} f_{\overline{R'R}_{\overline{X}_k}} = -f_{\overline{R'R}} \sin\left(\frac{\theta_p}{2} - \frac{\theta_r}{2}\right) \\ f_{\overline{R'R}_{\overline{Y}_k}} = -f_{\overline{R'R}} \cos\left(\frac{\theta_p}{2} - \frac{\theta_r}{2}\right) \end{cases} \quad (32)$$

$$\begin{cases} f_{\overline{R'S-X_k}} = f_{\overline{R'S}} \cos\left(\frac{\theta_p - 2\theta_r}{2}\right) \\ f_{\overline{R'S-Y_k}} = -f_{\overline{R'S}} \sin\left(\frac{\theta_p - 2\theta_r}{2}\right) \end{cases} \quad (33)$$

In analogy with Eqs. (32) and (33), the pressure forces acting on tooth space surface \overline{QP} are:

$$\begin{cases} f_{\overline{QO'-X_k}} = 2p_{in} \sin\left(\frac{\theta_r}{2}\right) b_k r_{ext} \sin\left(\frac{\theta_p}{2} - \frac{\theta_r}{2}\right) \\ f_{\overline{QO'-Y_k}} = -2p_{in} \sin\left(\frac{\theta_r}{2}\right) b_k r_{ext} \cos\left(\frac{\theta_p}{2} - \frac{\theta_r}{2}\right) \end{cases} \quad (34)$$

$$\begin{cases} f_{\overline{Q'P-X_k}} = -p_{in} (r_{ext} - r_k) b_k \cos\left(\frac{\theta_p - 2\theta_r}{2}\right) \\ f_{\overline{Q'P-Y_k}} = -p_{in} (r_{ext} - r_k) b_k \sin\left(\frac{\theta_p - 2\theta_r}{2}\right) \end{cases} \quad (35)$$

Finally, the global pressure force acting on an unbalanced tooth space can be obtained as the sum of the force components in Eqs (32-35). This pressure force, expressed in reference frame $O_k \overline{X_k Y_k}$, can be straightforwardly reduced in reference frame $O_k X_k Y_k$.

3.2 Pressure torques

The pressure torques are due to the pressure difference between the pressure in the tooth spaces of the meshing teeth which are the only unbalanced spaces (Figure 9). In the formulation of the PModel presented in [1], the pressure in the trapped volume was assumed as a linear decrease from the outlet to the inlet pressure and the pressure in the inlet and outlet chamber was assumed as constant. On the contrary, in this improved formulation, the trapped volume as well as the inlet and outlet chambers are assumed as control volumes and therefore their pressure field is calculated (see Sections 2.2, 2.3, 2.4). The pressure torque formulation is hereafter outlined for meshing contacts along the Direct Line of Action (DLA), while for meshing contact along the Inverse Line of Action (ILA), the reader can refer to [2]. In the case of one meshing contact, the pressure torque is calculated using the same expressions presented in the PModel (Eq (26) in [1]) but taking into account that, here, the pressure in the inlet and outlet chamber is time-varying

$$M_{pk} = b_k (p_{out} - p_{in}) \left(\frac{r_{ext}^2 - r_k^2}{2} \right) \quad (36)$$

In the case of two meshing contacts, one more term has to be taken into account, due to the pressure in the trapped volume (see Figure 9):

$$M_{pk} = (p_{out} - p_t) \left(\frac{r_{ext}^2 - r_k^2(t)}{2} \right) b_k + (p_t - p_{in}) \left(\frac{r_{ext}^2 - r_k^2(t+T)}{2} \right) b_k \quad (37)$$

It is worth noting that pressure torque M_{pk} is a function of time, because radial distances r_1, r_2 depend on time as well as on p_{in}, p_{out} and p_t .

4. EXPERIMENTAL VALIDATION AND SIMULATION RESULTS

4.1 Experimental validation

The validation is carried out using the same methodology described in Section 4 of Part III, but using in the simulation process the improved pressure forces and torque. The simulation results are carried out by using the same data used in Part III. Hereafter the results in the time and frequency domain are presented.

The time synchronous average (TSA) of the experimental quantity on the left side of Eqs. (42-44) of Part III was computed over 250 meshing periods at 2000 rpm, 300 meshing periods at 2600 rpm and 400 meshing periods at 3350 rpm, while the TSA of the simulation quantity (on the right side) was computed over 48 meshing periods. Figure 10 to Figure 12 show the comparison between the root mean square (RMS) values of the experimental quantity and the simulation results, concerning the *NModel* and the *PModel*. It can be noted that the new model is able to achieve results closer to the experimental data than the previous model, in particular in X_1', Y_1' and θ_1' directions at 34 bar (see Figures 2a and 8 in Part III for the reference frame). At 90 bar the RMS values of the TSA for the new and previous model give similar results. The validation results in frequency domain are shown in Figure 13 to Figure 15, where the amplitude of the spectra of the experimental quantity are compared with the spectra obtained using the new model. Taking as reference the waterfall maps of the previous model (Figure 10, 11 and 12 of Part III) it can be noted that the agreement in θ_1' -direction is the same at both pressures, while in X_1' and Y_1' -directions the agreement is better for the *NModel*. In

X_1' -direction and 90 bar the experimental resonances at about 2.5 and 5.2 kHz can be seen in the simulated map (Figure 13). In Y_1' -direction the experimental resonances at 2.5 and 4.2 can be found in the model map (Figure 14) both at 34 and 90 bar. Therefore, the validation results both in time and frequency domain can be considered better for the new model. Nevertheless, the improved pressure formulation has been developed with a double objective: on the one hand in order to better match the experimental data, and on the other hand in order to clearly understand the pressure phenomena occurring in the gear pump, as the pressure ripple.

4.2 Comparing the results of the two formulations

In the following the results of the integration of the differential equation system (29) are compared with the results obtained using the *PModel* in order to highlight the introduced improvements. The comparisons is carried out in terms of pressure distribution, pressure forces and torques acting on gears.

The results related to the pressure distribution comparisons concern a pump operating in a typical working condition in terms of operational pressure and gear speed: namely 34 bar and 2000 rpm. The pressure distribution around the gears represents the pressure inside a tooth space during a complete rotation of the gears, i.e. while the tooth space moves itself from the low to the high pressure chamber. Figure 16 shows the comparison in terms of pressure distribution in the isolated volumes between the *PModel* and the *NModel*. In particular the pressure distribution represented in Figure 16 starts when the first tooth space becomes isolated at the inlet side and end when the last isolated tooth space begins the communication with the outlet chamber and consequently the number of isolated tooth spaces is reduced by one. It can be noted that the improved pressure distribution shows several oscillations that correspond to the number of isolated tooth spaces, while the previous one does not show such a phenomenon because of the poor modelling. Moreover, the increase of the pressure in the first isolated tooth spaces is smoother in the improved pressure and postponed than in the previous model mainly due to the new axial flow rate through the clearance between bearing block and casing internal surface. It is interesting to note that Refs. [5][6] present some experimental measurements of the pressure distribution in a gear pump similar to the gear pump being studied in this work. The measurement results depict the same trend of the pressure distribution estimated by the *NModel*, in particular showing the pressure ripples similar to those in Figure 16. Figure 17 shows the pressure distribution in the outlet chamber for the new model and for the previous model. It can be noted that in the previous model the pressure in the outlet chamber (as in the inlet chamber) was taken as constant while in the model described here, both the inlet and outlet chamber have been considered as control volumes (see Section 2.3). The improved pressure distribution shows the pressure oscillations due to the volume variation of the chamber and due to the communication with the adjacent control volumes. Figure 18 shows the pressure distributions in the trapped

volume. It can be noted that the pressure variations are similar, however the pressure decrease is smoother for the new model. In fact, it is interesting to note that in the *PModel*, the pressure in the trapped volume was assumed as a linear decrease from the outlet to the inlet pressure and the pressure in the inlet and outlet chamber was assumed as constant; this lead to a pressure variation in the trapped volume (Fig 18) very sharp.

The comparison in terms of pressure forces and torque has been carried out at the operational pressure of 90 bar and at the operational speed of 2000 rpm. Figure 19 shows the pressure forces acting on both gears estimated by the two mentioned models. It can be seen that the trends are similar and both models capture the sudden variations in correspondence to some events which occur during the meshing phase, such as change in the number of isolated volumes carrying fluid, and in the trapped volume connections. Important variations are due to phenomena concerning the trapped volume, occurring when its connection with the inlet begins at about 16% of T , and when its connection with the outlet ends at about 20% of T . Another large variation takes place when the number of isolated tooth spaces increases from 6 to 7, at about 25% of T for gear 1 and 75% of T for gear 2 (see also Fig. 4); in this instant a new space becomes isolated from the input chamber and its pressure undergoes a sudden increment. On the contrary, the force variation is small when the number of the isolated tooth spaces decreases from 7 to 6, that is to say, when an isolated space begins to be opened to the output chamber, at about 61% of T for gear 1 and 12% of T for gear 2. In this case, the force variation is small since its pressure is already near the output pressure. It is interesting to note that the pressure forces estimated by the new model are smoother in correspondence of these sudden variations with respect to the forces estimated by the *PModel*. Such a behaviour is mainly due to the improved modelling of the trapped volume. Finally, Figure 20 depicts the comparison between the pressure torque acting on both gears estimated by the new and the previous model. As expected, the trend of the pressure torque calculated by the new model is smoother in the location where the sudden variations related to the trapped volume connections (between 16% and 20% of T) happen. Furthermore, the improved pressure torque behaviour can capture the little variation due to the end of the existence of the trapped volume (vertical dotted line in Figure 20). Thus, the improved modelling of the phenomena bound to the trapped volume plays an important role in the estimation of the dynamic forces and torque.

5 CONCLUDING REMARKS

The previously presented model of gear pump was modified with the aim of improving the calculation of pressure forces and torques in order to better understand the pressure phenomena acting on this kind of device and also in order to achieve a behaviour closer to the real measurements. In this sense, the improved pressure formulation includes several phenomena not considered in the previous one, such as the pressure variations at input and output ports, the

axial flows through the clearances between floating bushes and case as well as an accurate description of the trapped volume and its connections with high and low pressure chambers. Moreover, in the new formulation, the pressure around the gears was simultaneously estimated for both gears. The improved model is able to achieve results closer to the experimental data than the previous model, in particular, in the time domain comparison. Moreover, the new model can simulate pressure phenomena occurring in the gear pump such as the pressure ripple. As a matter of fact, thanks to the new formulation, the simulation results of the improved pressure evolution in the isolated tooth spaces show pressure oscillations that correspond to the isolated tooth spaces, while the previous model does not show such phenomenon because of the simpler modelling. In the previous model (Part I) the pressure in the outlet chamber (as in the inlet chamber) was taken as constant while in the model described here, both the inlet and outlet chambers have been considered as control volumes and the improved pressure distribution shows the pressure oscillations due to the variation in volume of the chamber and due to the communication with the adjacent control volumes. It is important to underline that the improved pressure distribution shows the same trend as the experimental results in [5]. The originality of this paper concerns the development of a non-linear model of gear pumps that implements formulations about pressure distribution, hydrodynamic bearing forces and meshing stiffness. In particular, it is original to include all these important dynamic effects in the same model, in order to take into account their interactions. This can be important in order to foresee the influence of working conditions and design modifications on vibration and noise generation. Thus, the model could be a very useful tool in prototype design and in design optimisation in order to identify the origin of unwanted dynamic effects.

ACKNOWLEDGEMENTS

The authors wish to thank TRW Automative Italia S.r.l. – Division Automotive Pumps (Ostellato, Ferrara, Italy) and the engineers of this Company for co-operation and assistance in the collection of model data. This work has been developed within the Advanced Mechanics Laboratory (MechLav) of Ferrara Technopole, realized through the contribution of Regione Emilia-Romagna - Assessorato Attivita' Produttive, Sviluppo Economico, Piano telematico - POR-FESR 2007-2013, Attività I.1.1..

References

- [1] E. Mucchi, G. Dalpiaz, A. Fernández del Rincón, Elasto-dynamic analysis of a gear pump. Part I: pressure distribution and gear eccentricity, *Mechanical Systems and Signal Processing* 24 (2010) 2160-2179.
- [2] E. Mucchi, G. Dalpiaz, A. Rivola, Elasto-dynamic analysis of a gear pump. Part II: Meshing phenomena and simulation results, *Mechanical Systems and Signal Processing* 24 (2010) 2180-2197.

- [3] H. Kuang, Y. T. Yang, An estimate of mesh stiffness and load sharing ratio of a spur gear pair, ASME, International Power Transmission and Gearing Conference, Vol 1, 1992.
- [4] Childs D., Moes H., Van Leeuwen H., Journal bearing impedance descriptions for rotordynamic application. Transactions of the ASME, 1977.
- [5] G. Miccoli, P. Vagnoni, Experimental determination of casing loads on an external gear pump, *Oleodinamica-pneumatica*, Novembre 1988, 145-155, (in Italian).
- [6] Mancò S., Nervegna N., Pressure transient in an external gear hydraulic pump, *Fluid power*, Edited by T. Maeda, 1993.
- [7] K.J.Huang, W.C. Lian, Kinematic flowrate characteristics of external spur gear pumps using an exact closed solution, *Mechanism and Machine theory* 44 (2009) 1121-1131.
- [8] R. Castilla, J. Wojciechowski, P.J. Gamez-Montero, A. Vernet, E. Codina, Analysis of the turbulence in the suction chamber of an external gear pump using time resolved particle image velocimetry, *Flow Measurements and Instrumentation* 19 (2008) 377-384.
- [9] G. Houzeaux, R. Codina, A finite element method for the solution of rotary pumps, *Computers and fluids* 36 (2007) 667-679.
- [10] R. Castilla, J. Wojciechowski, P.J. Gamez-Montero, A. Vernet, E. Codina, "Analysis of the turbulence in the suction chamber of an external gear pump using Time Resolved Particle Image Velocimetry", *Flow Measurement and Instrumentation* 19 (2008) 377-384.
- [11] M. Eaton, K. Edge, Modelling and Simulation of Pressures within the Meshing Teeth of Gear Pumps, *Proceedings of Conference on Recent Advances in Aerospace Actuation Systems and Components*, (2001) 21-26.
- [12] D. Fielding, C.J. Hooke, K. Foster, M.J. Martin, Sources of Pressure Pulsation from a Gear Pump, *Quiet Oil Hydraulic Systems*, (1977) 69-80.
- [13] N.D. Manring, S.B. Kasaragadda, The Theoretical Flow Ripple of an External Gear Pump, *Journal of Dynamic Systems, Measurement and Control*, 125 (2003) 396-404.
- [14] A. Vacca, S. Dhar. T. Opperwall. A coupled lumped parameter and CFD approach for modelling external gear machines, *Proceedings of 12th Scandinavian International Conference on Fluid Power*, 3 (2011) 161-178.
- [15] C. Bonacini and M. Borghi, Calculation of the pressure in the vanes between teeth of an external gear pump, *Oleodinamica-pneumatica*. Novembre 1991, 128-134, (in Italian).
- [16] S. Mancó, N. Nervegna, A mathematical model of external gear pumps, *Oleodinamica-pneumatica* 1/87 (1987) 64-72, (in Italian).
- [17] I.E. Idelchik, *Handbook of hydraulic resistance*, 3rd Edition, 2001.

FIGURES

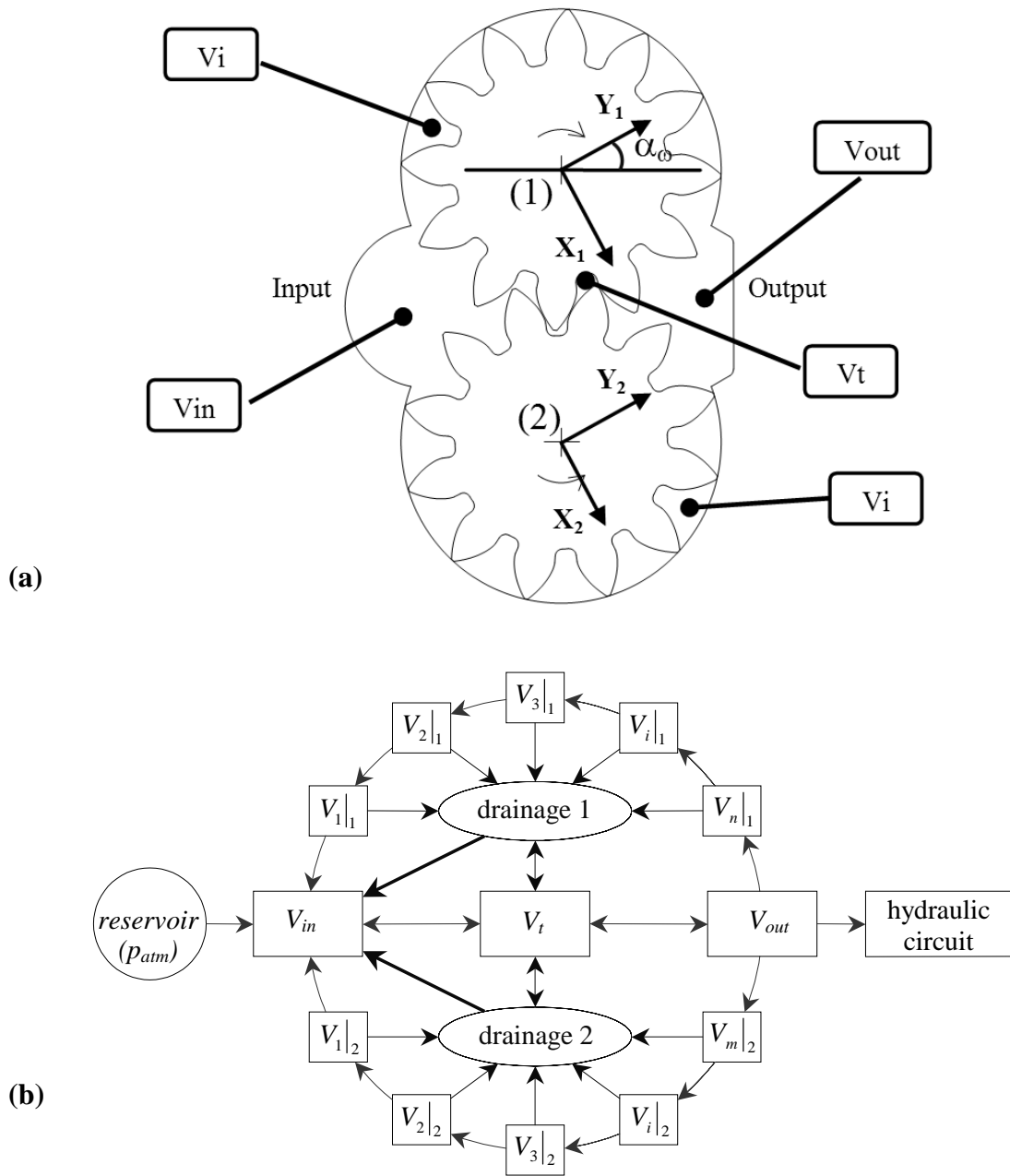
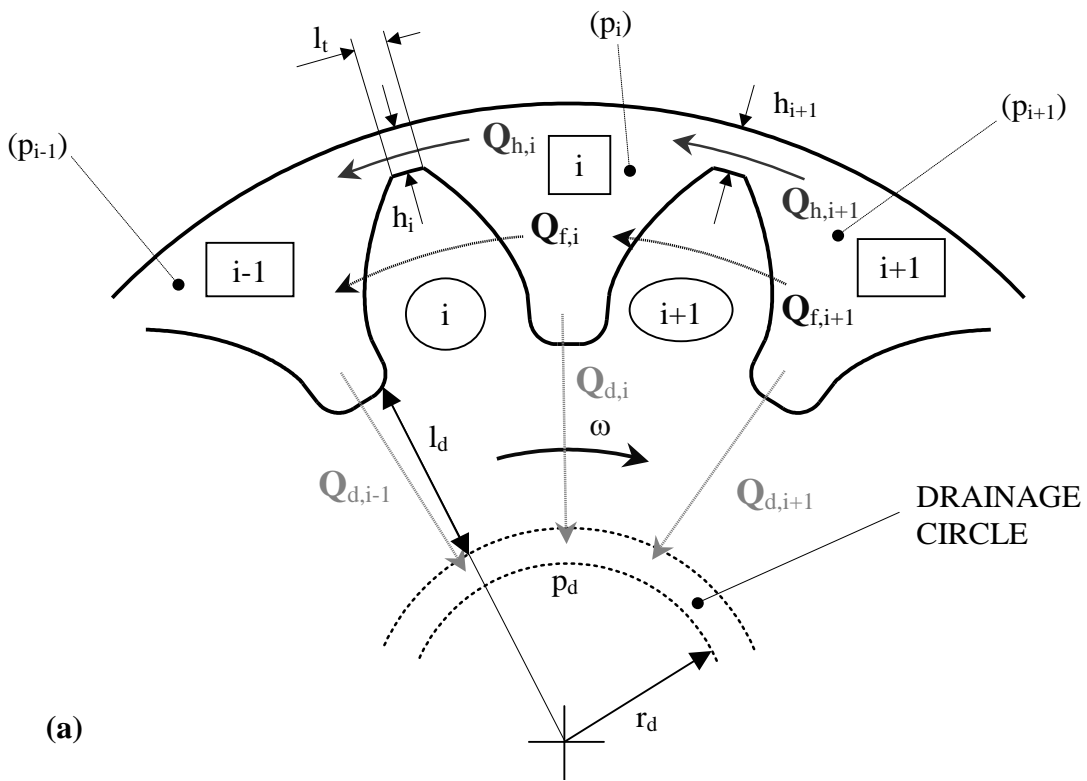
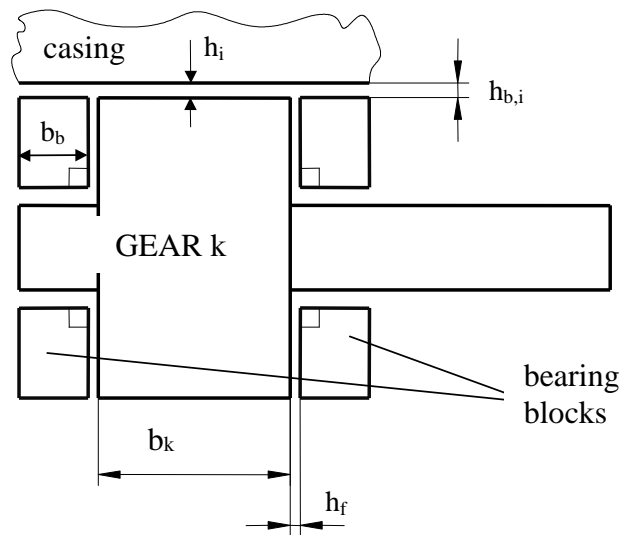


Figure 1. (a) Control volumes and (b) relating flows. Gear 1 is the driving gear, gear 2 is the driven gear.



(a)



(b)

Figure 2. a) Volumetric flow rates for the generic tooth space i and b) clearances between pump components

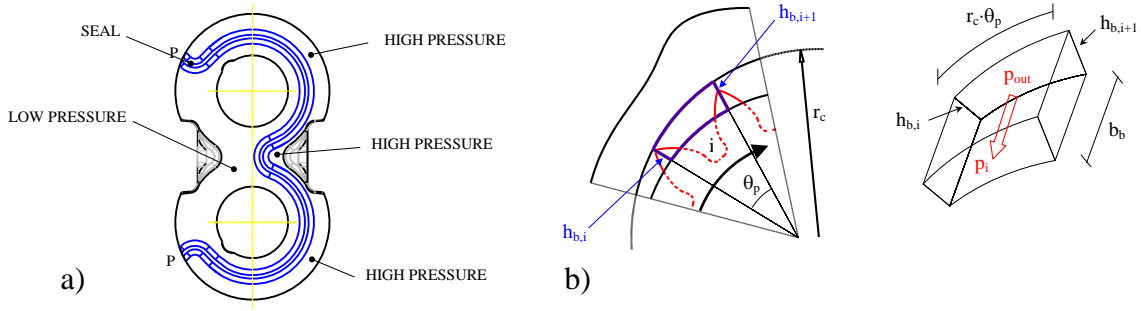
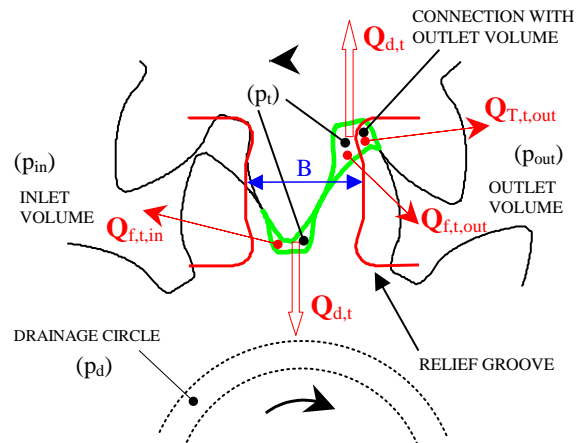


Figure 3. a) Balancing seal in the bearing block surface and b) axial flow rate through the clearance between casing and bearing block when the tooth space is beyond point P.

a)



b)

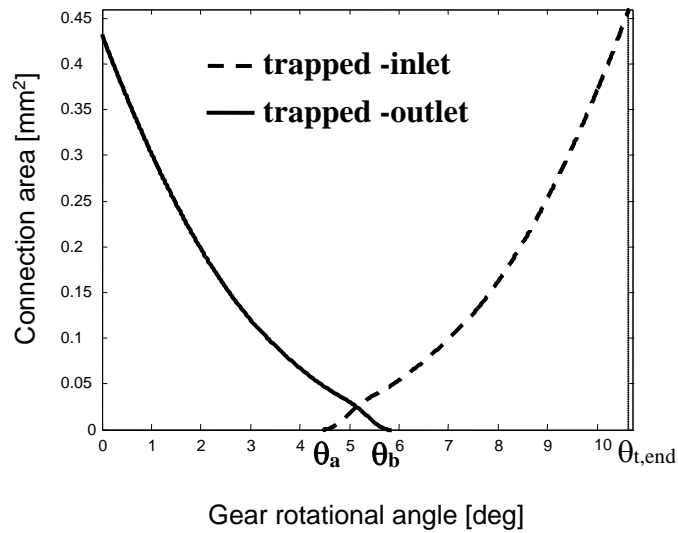
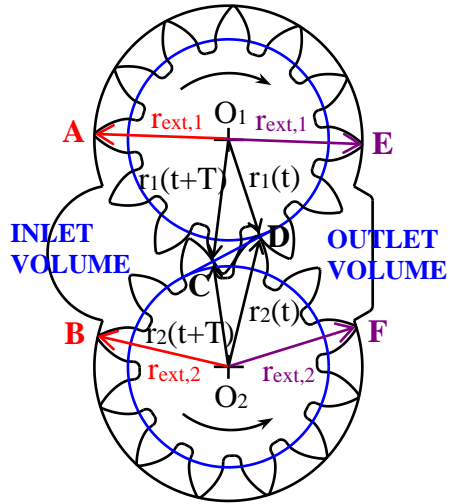


Figure 4: a) Volumetric flow rates for the trapped volume (the flow rate $Q_{T,t,in}$ is not depicted because in such a gear configuration the connection with the inlet volume does not exist) and b) connection area between the trapped volume and the inlet (in dotted line) and the outlet (in solid line) volumes.

a)



b)

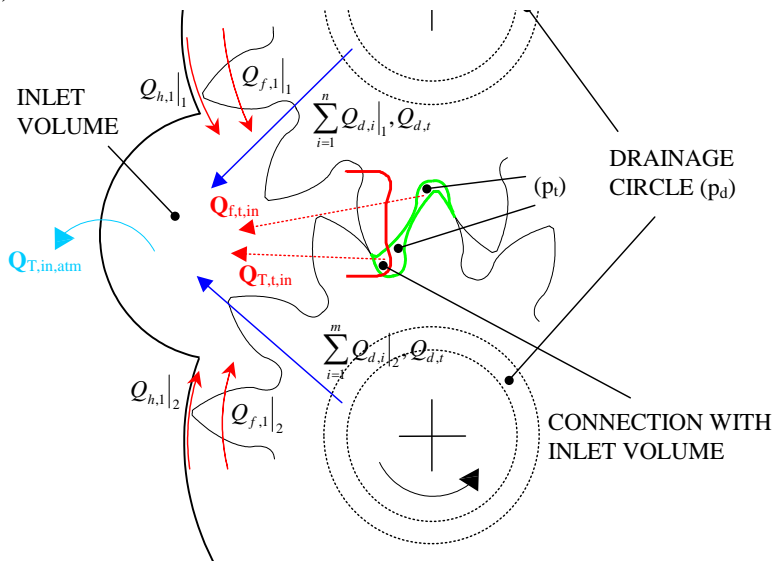


Figure 5. a) Schematic for the calculus of the control volumes and their variations and b) Volumetric flow rates for the inlet volume

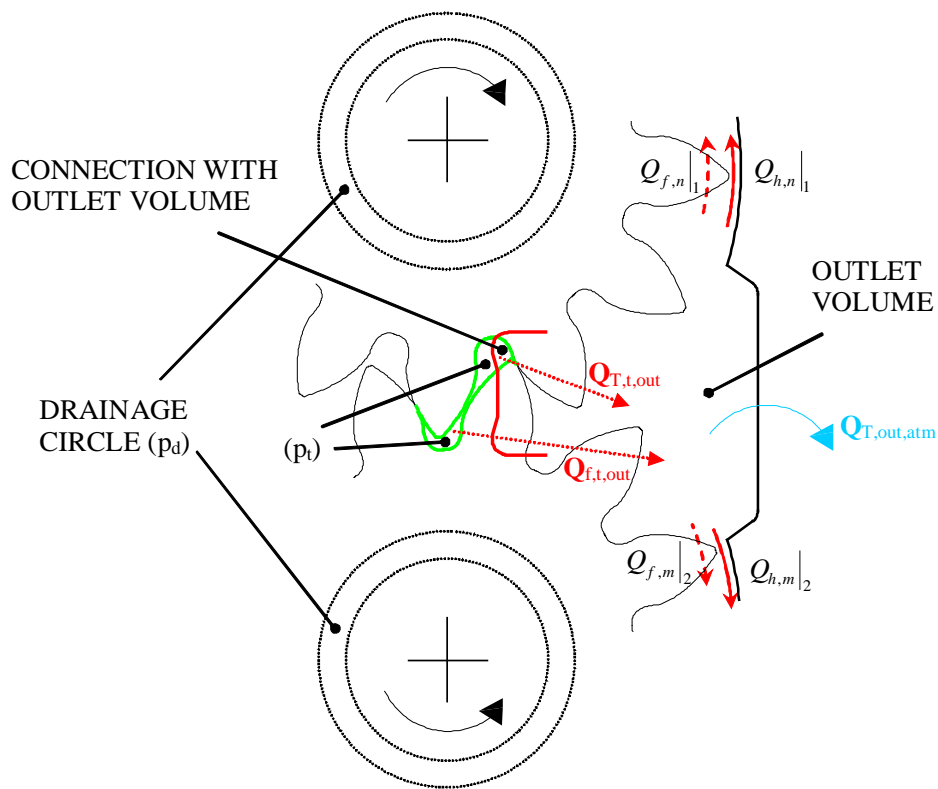


Figure 6. Volumetric flow rates for the outlet volume.

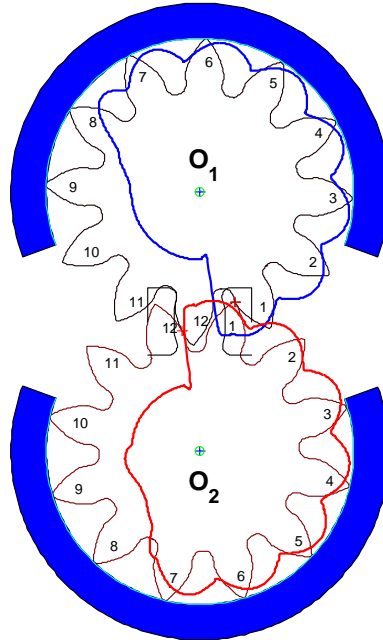


Figure 7. Pressure evolution in a tooth space of gear 1 and 2 for a complete rotation at the operational condition of 2000 rpm and 34 bar, represented in polar coordinates.

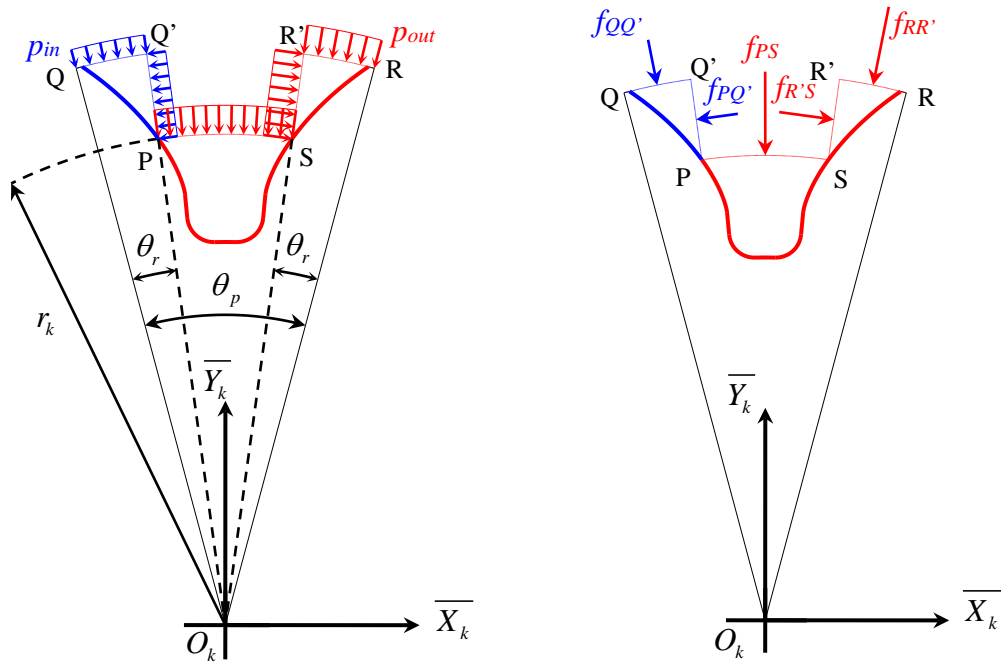


Figure 8. Pressure force in a not balanced tooth space of gear 2; P is the point where the contact between teeth takes place.

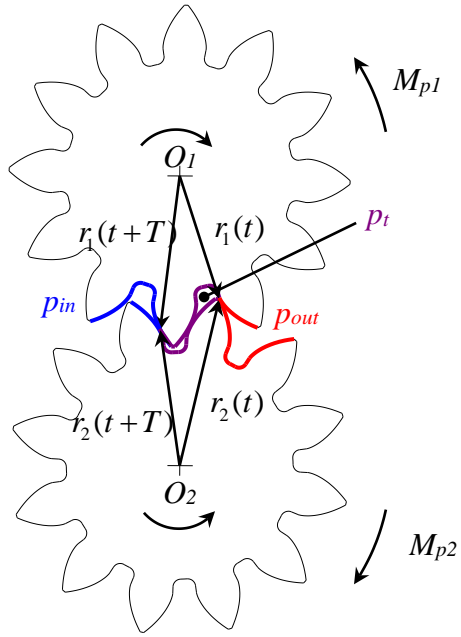


Figure 9. Not balanced tooth space in case of two meshing contacts.

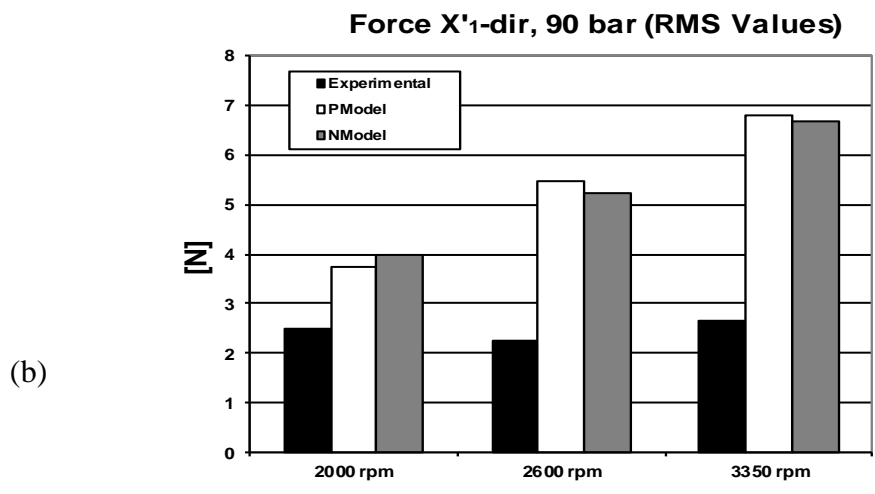
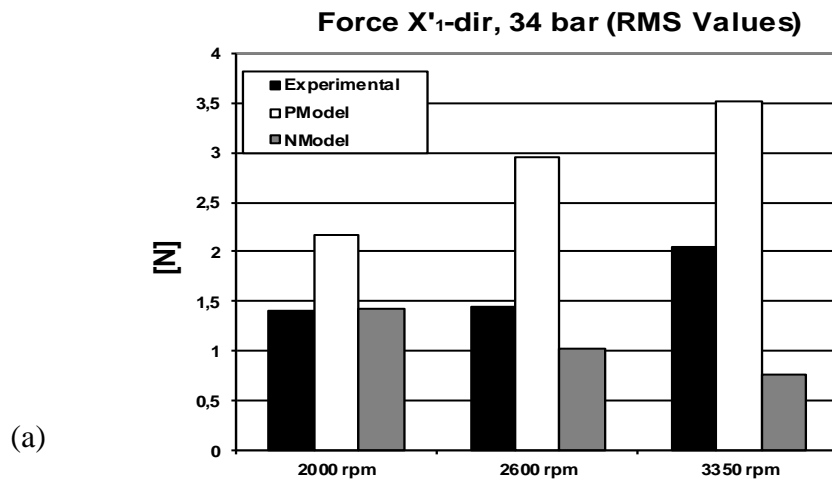


Figure 10. RMS values of the TSA relative to one meshing period of the force in X_1' -direction: (a) at 34 bar and (b) at 90 bar.

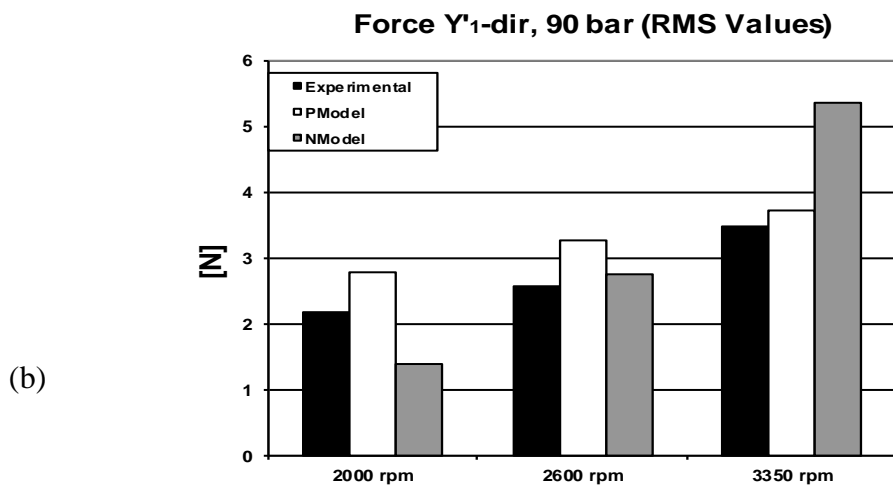
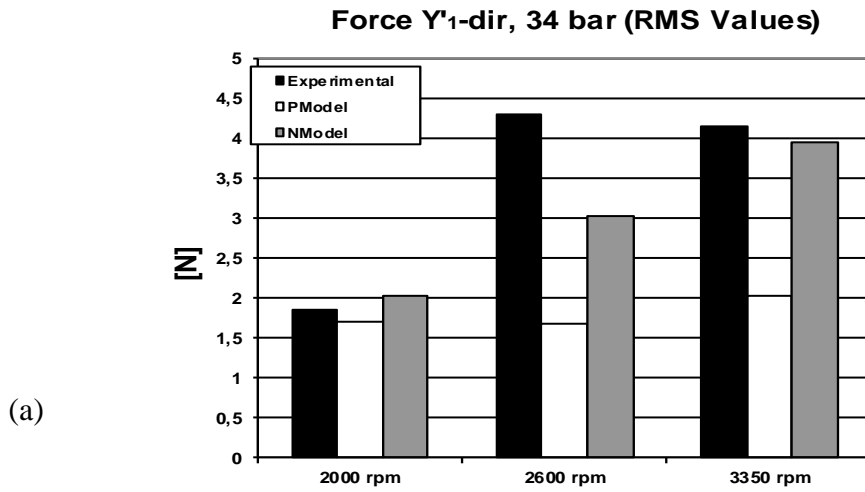


Figure 11- RMS values of the TSA relative to one meshing period of the force in Y_1' -direction: (a) at 34 bar and (b) at 90 bar.

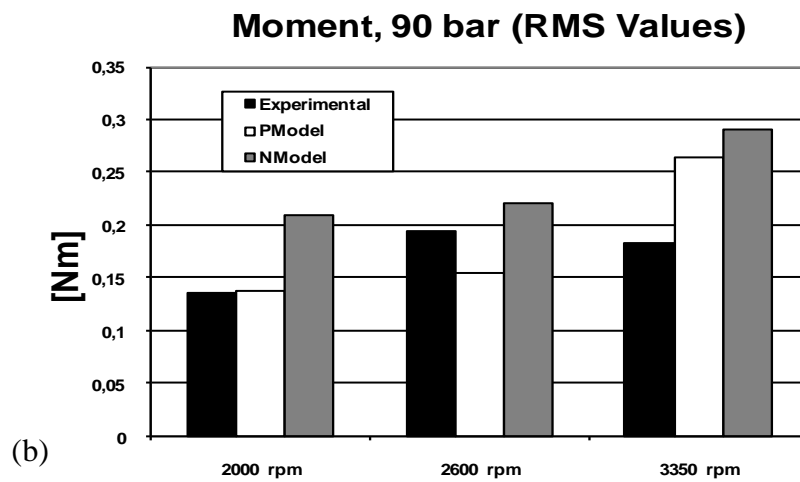
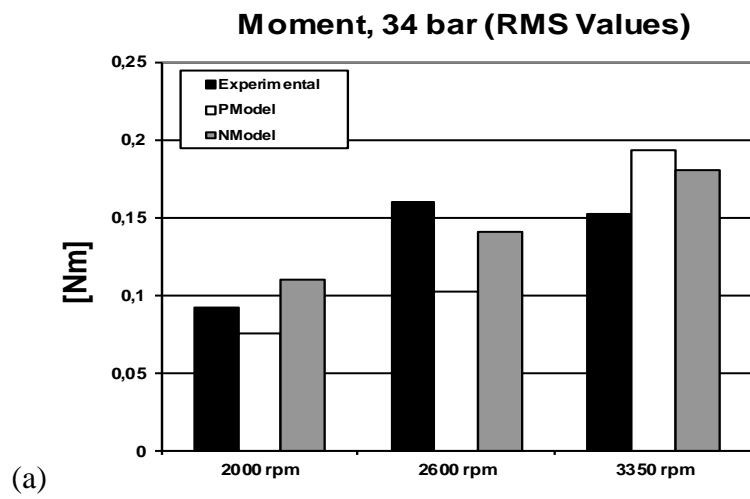


Figure 12. RMS values of the TSA of the moment (θ_1' -direction) relative to one meshing period: (a) at 34 bar and (b) at 90 bar.

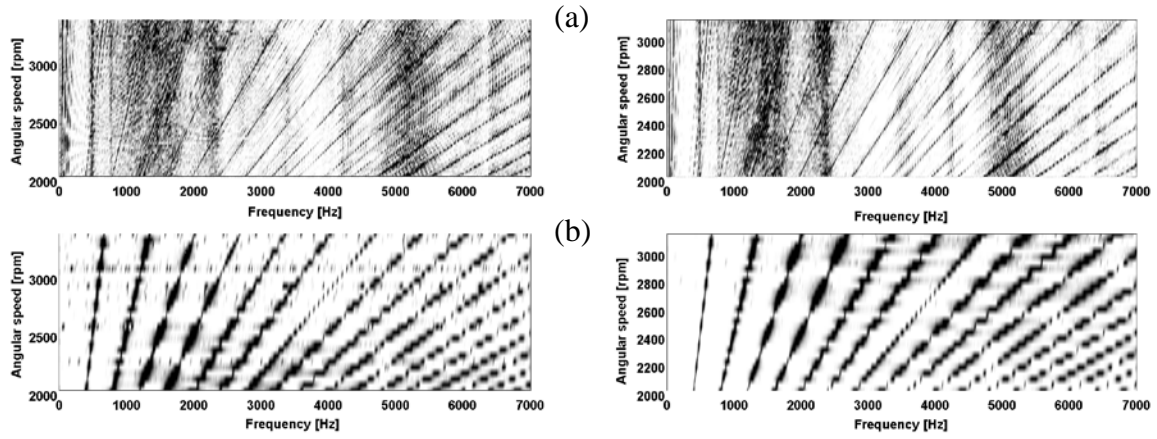


Figure 13. Waterfall maps of force spectra in X_1 -direction at 34 bar (left) and 90 bar (right); according to the experiment (a) and simulation (b).

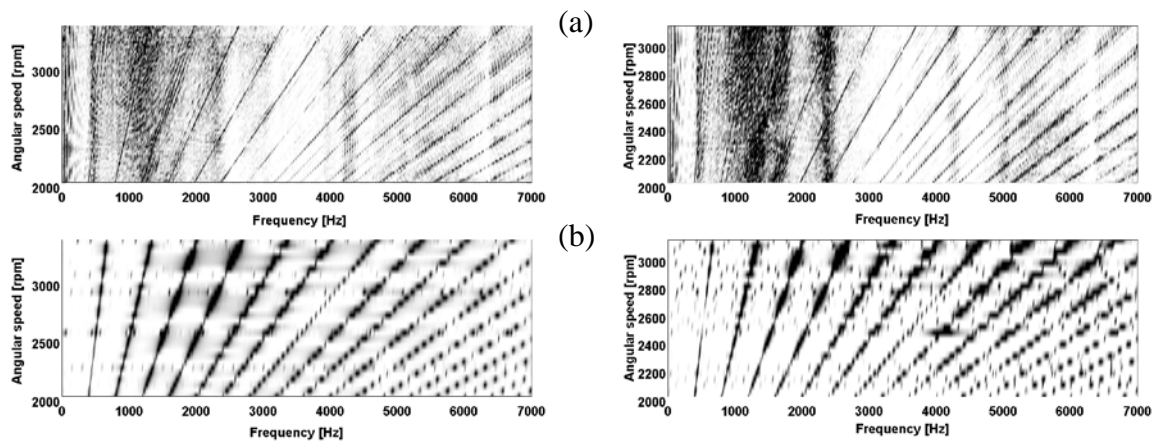


Figure 14. Waterfall maps of force spectra in Y_1' -direction at 34 bar (left) and 90 bar (right); according to the experiment (a) and simulation (b).

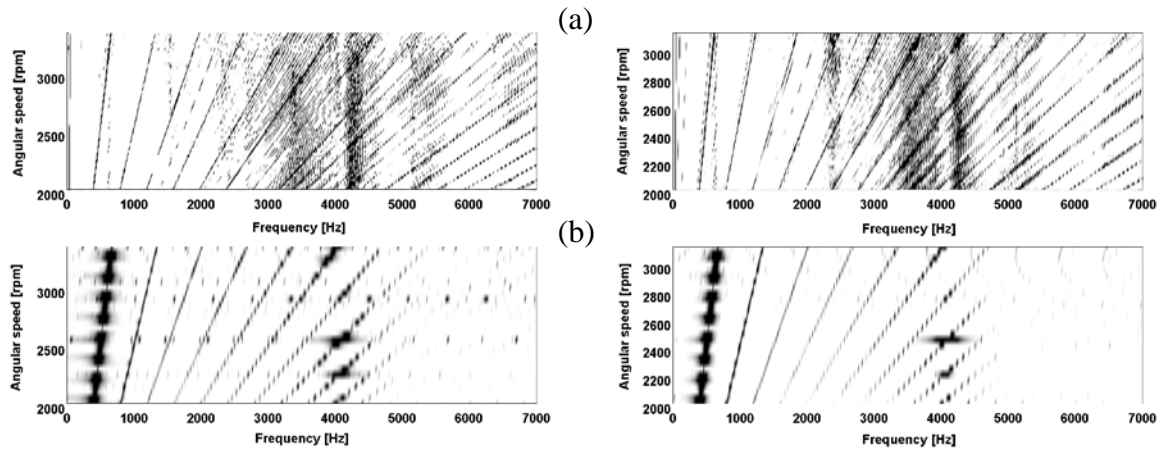


Figure 15. Waterfall maps of moment spectra (θ'_1 -direction) at 34 bar (left) and 90 bar (right); according to the experiment (a) and simulation (b).

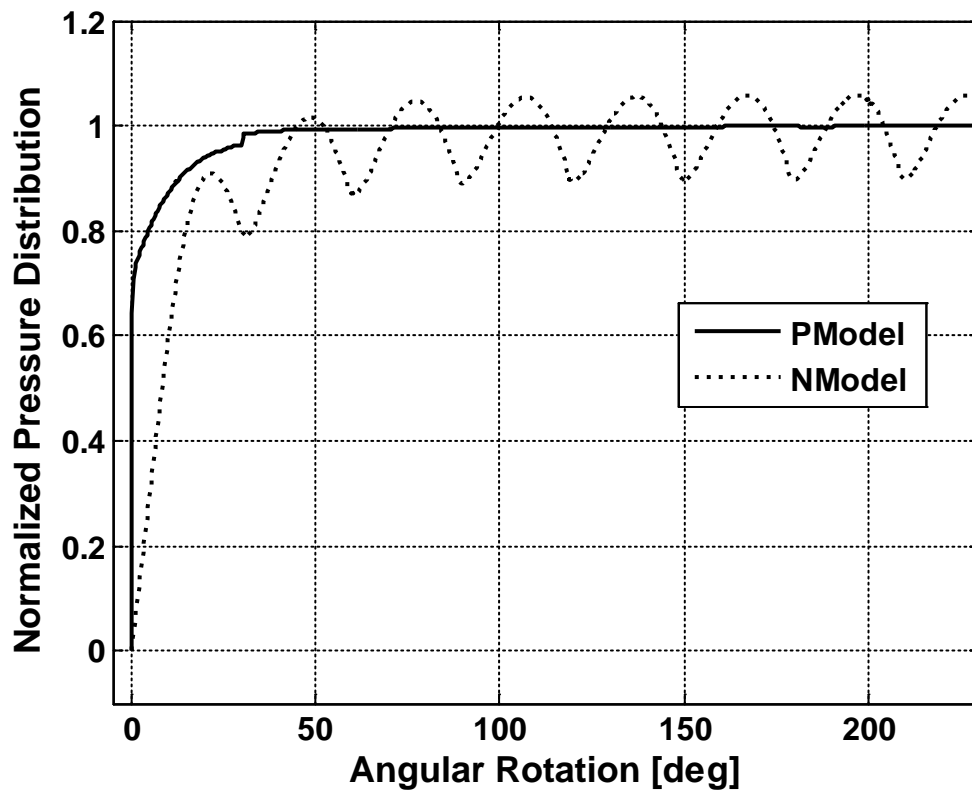


Figure 16. Pressure evolution in the isolated tooth spaces for gear 1 at the operational condition of 2000 rpm and 34 bar. Comparison between *PModel* and *NModel*.

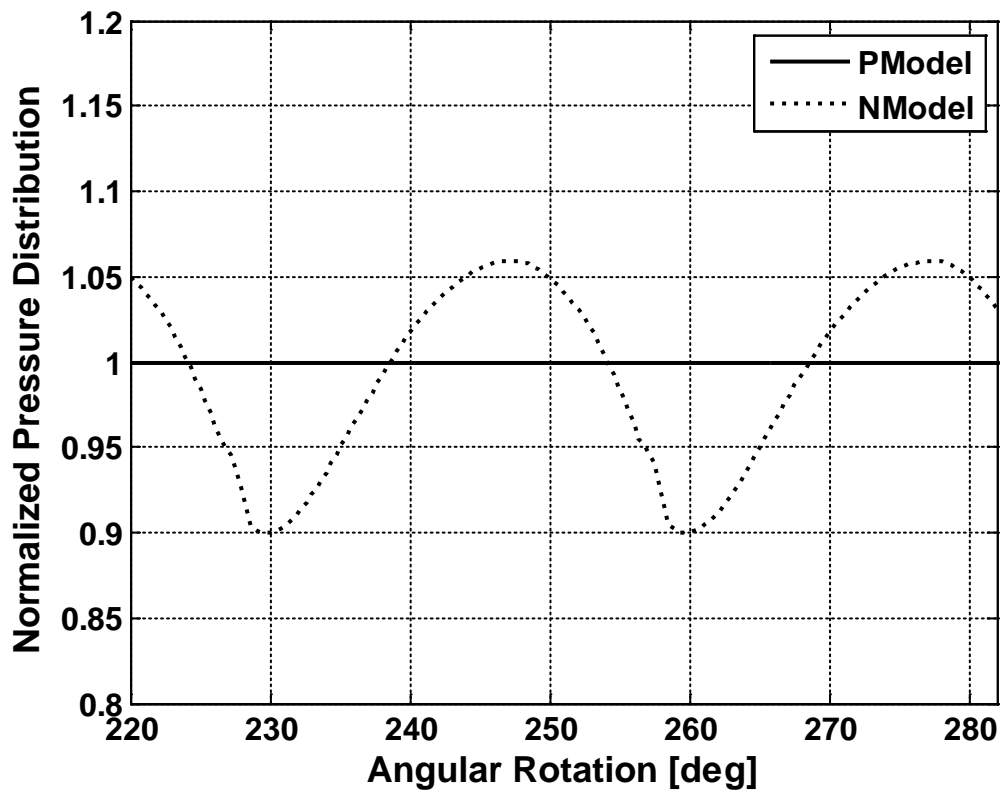


Figure 17. Pressure evolution in the outlet volume for gear 1 at the operational condition of 2000 rpm and 34 bar. Comparison between *PModel* and *NModel*.

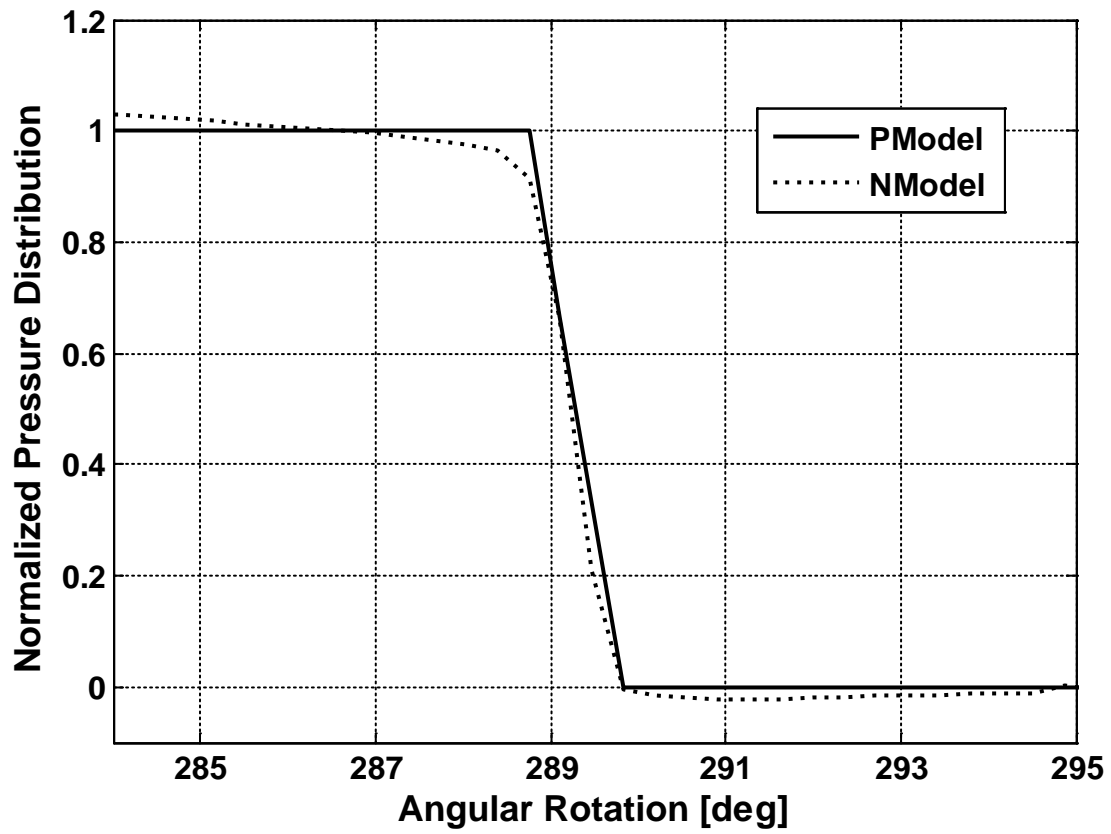


Figure 18. Pressure evolution in the trapped volume for gear 1 at the operational condition of 2000 rpm and 34 bar. Comparison between *PModel* and *NModel*.

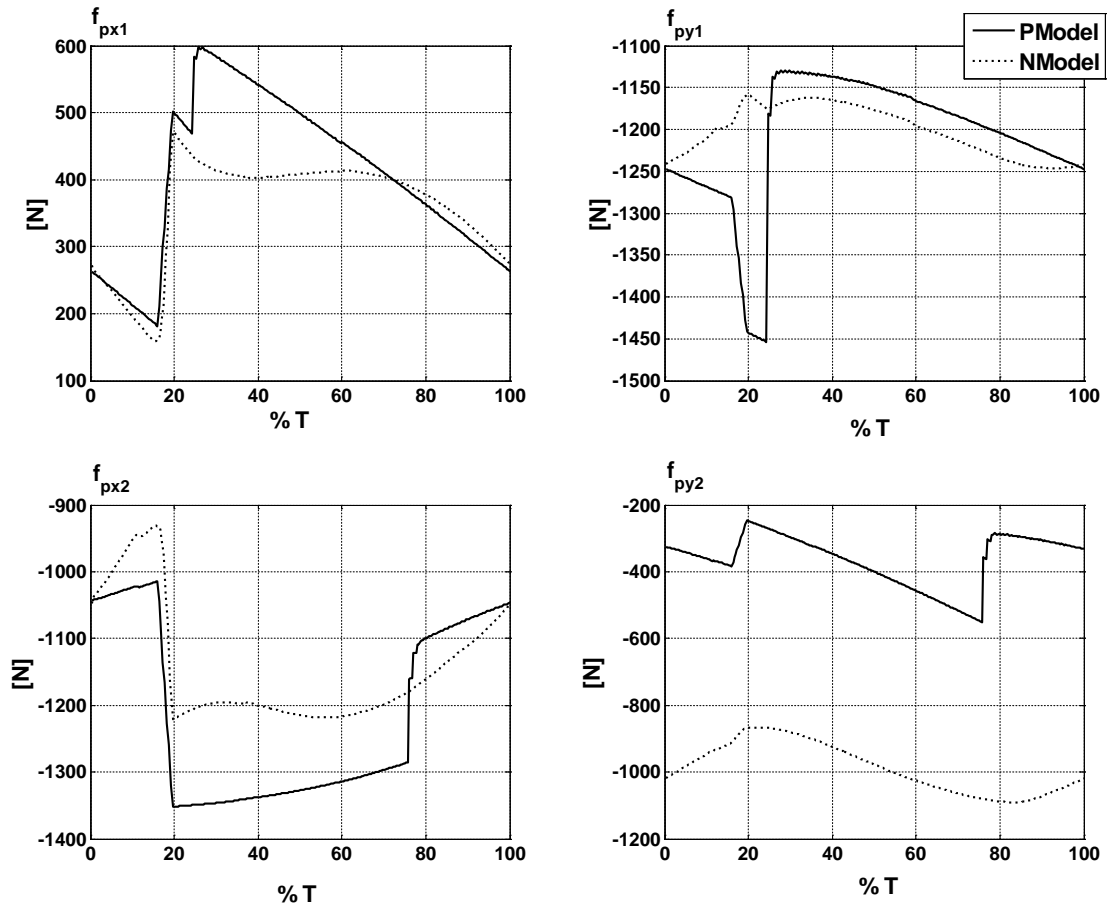


Figure 19. Evolution of the pressure forces over one meshing period in the reference frame $O_k X_k Y_k$ at the operational condition of 2000rpm and 90bar. Comparison between *PModel* and *NModel*.

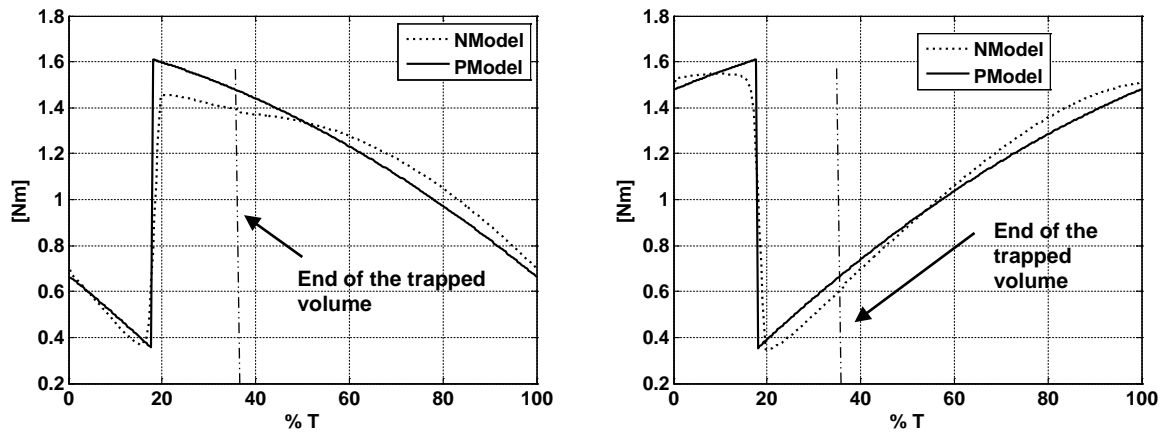


Figure 20. Pressure torques acting on gears over one meshing period at the operational condition of 2000rpm and 90bar, starting from the position when the second tooth pair comes into contact. The vertical dotted line defines the end of the trapped volume, corresponding to the angular rotational of $\theta_{t,end}$ (see Figure4b).

Comparison between PModel and NModel.

TABLES

Table 1: Number of control volumes as a function of rotational angle. The starting position is when a new meshing begins.

	From→To					
	$\theta_0 \rightarrow \theta_1$	$\theta_1 \rightarrow \theta_2$	$\theta_2 \rightarrow \theta_3$	$\theta_3 \rightarrow \theta_4$	$\theta_4 \rightarrow \theta_5$	$\theta_5 \rightarrow \theta_p = \theta_0$
Rotational angle[deg]	3°11'	4°22'	3°11'	7°27'	4°22'	7°27'
# of trapped volumes	1	1	1	0	0	0
# of isolated tooth space volumes (gear 1)	6	6	7	7	6	6
# of isolated tooth space volumes (gear 2)	7	6	6	6	6	7
# of inlet and outlet volumes	2	2	2	2	2	2
Total number of control volumes	16	15	16	15	14	15